Role of dynamin in elongated cell migration in a 3D matrix

Justin G. Lees[*], Nick N. Gorgani[†], Alaina J. Ammit[‡], Adam McCluskey[§], Phillip J. Robinson[†], Geraldine M. O'Neill[*,‖]

[*]Children's Cancer Research Unit, Kids Research Institute, The Children's Hospital at Westmead, Westmead, New South Wales, Australia, [†]Children's Medical Research Institute, The University of Sydney, Westmead, New South Wales, Australia, [‡]Faculty of Pharmacy, The University of Sydney, Sydney, New South Wales, Australia, [§]Faculty of Chemistry, School of Environmental and Life Sciences, The University of Newcastle, Callaghan, New South Wales, Australia. [‖]Discipline of Paediatrics and Child Health, The University of Sydney, Sydney, New South Wales, Australia.

*Corresponding Author:
Geraldine M. O'Neill
Children's Cancer Research Unit
Kids Research Institute
The Children's Hospital at Westmead
Locked Bag 4001, Westmead, 2145
Australia
Ph: 61 2 9845 1206
Fax: 61 2 9845 3078
Email: geraldine.oneill@health.nsw.gov.au

Running title – Dynamin and elongated 3D migration.

Abbreviations – 3-dimensional (3D)

Abstract

The use of 3-dimensional (3D) collagen gels has yielded new insights into the migratory behaviour of cancer cells. While the large GTPase dynamin has emerged as an important regulator of cancer cell migration and invasion under 2D conditions, its role in 3D migration is unclear. We have used a potent dynamin modulator, a bis-tyrphostin derivative, Ryngo® 1-23, to investigate the role of dynamin in 3D migration in 3 different cell lines. The compound specifically inhibits persistent, elongated 3D migration in U87MG and SMA-560 cells. Treated U87MG cells adopt a rounded morphology that is not due to apoptosis, loss of matrix metalloprotease activity or inhibition of clathrin-mediated endocytosis. Given that Ryngo 1-23 is known to regulate dynamin oligomerisation and actin dynamics at the leading edge, we analyzed actin filament distribution. Ryngo 1-23 induced a switch in actin filament organization in 3D cultures resulting in the generation of multiple short actin-rich microspikes. Correlated with the change in actin filament distribution, cells displayed reduced collagen gel contraction. Since acto-myosin force transmission to the extra-cellular matrix underpins persistent, elongated migration, our results suggest that Ryngo 1-23 modulates this process in 3D migration via dynamin-mediated regulation of acto-myosin force transmission to the extra-cellular matrix.

1. Introduction

The progression to invasive, metastatic disease remains a major impediment to the successful treatment of cancer. Thus there have been intensive research efforts to identify the molecules and mechanisms that underpin the migratory ability of invasive cancer cells. While much work has been done using cells grown on planar 2-dimensional (2D) surfaces, it is increasingly realized that the 3D tissue structure surrounding cancer cells *in vivo* is an important determinant of cell migration behaviour [1-4]. Therefore the use of 3D culture models imparts important physiological insights into cancer cell migration. The large GTPase dynamin has emerged as an important regulator of cancer cell invasion [5], but to date the role that this protein plays in the negotiation of a 3D tissue architecture is not understood.

In a 3D matrix cells must generate contractile force through their actin cytoskeleton, transmit this force via adhesion to the matrix and then either deform themselves in order to squeeze through pores in the matrix, or alternatively, secrete proteases to degrade the matrix and thereby create space for the cell body [6]. The greater the adhesion force the cell can transmit to the surrounding matrix the faster they can move through the 3D matrix and the greater their directional persistence [7]. In the transition zone between the lamellipodia and the lamella where focal adhesions form, a molecular clutch has been proposed to form between the focal adhesions and the actin filaments [8]. This clutch facilitates acto-myosin force transmission to the extra-cellular matrix and thus regulates forward cell movement. Cancer cells characteristically adopt different morphologies reflecting their response to the constraints imposed by a 3D matrix [1, 2]. The two most commonly described morphologies are an elongated/mesenchymal cell shape versus a rounded/amoeboid cell shape. During elongated cell migration, cells secrete matrix metalloproteases and pull themselves forward by attaching to matrix fibres. In contrast, rounded invasion is considered to be adhesion-independent and depends on a highly contractile acto-myosin cytoskeleton that produces membrane blebs which allow cells to squeeze through pores in the matrix.

In addition to these well-described 3D invasion behaviours (and other alternative modes [9]) we showed that rounding can be induced by elevated expression of the actin accessory protein tropomyosin Tm5NM1 [10, 11]. This induces a prominent change in the organization of actin filaments in 3D, with cells displaying multiple actin-rich microspikes that align with the surrounding matrix fibres. Following elevated Tm5NM1 expression leading to cell rounding and microspike formation, cells become non-motile. Thus actin filament organization in 3D culture conditions reflects different cellular motility outcomes.

Functional dynamin GTPase is formed via the association of subunits in a tetramer that further organizes into a helical polymer [5]. The tetramer structure facilitates dynamin interaction with the neck of clathrin-coated pits during vesicle endocytosis. Dynamin oligomers also associate with, and elongate, actin filaments [12, 13]. Correspondingly, many studies show that dynamin plays a role in actin cytoskeletal dynamics [5, 14, 15]. Recent studies suggest that dynamin 2 may regulate the molecular clutch at the leading edge of motile cells [16]. Reducing dynamin function by siRNA-mediated depletion, dominant negative dynamin II expression and dynamin chemical inhibitors (dynasore and myristyl trimethyl ammonium bromide (MiTMAB™)) all reduce 2D cell migration and transwell matrigel invasion [17, 18]. Dynamin also regulates the endocytic delivery of membrane-type matrix metalloproteinase 1 to the cell surface, for the conversion of the pro-form of the matrix-metalloprotease MMP-2 to active MMP-2 [19] that is important for elongated cell

migration in 3D culture. Endocytosis-mediated turnover of focal adhesions to the extracellular matrix and actin filament dynamics are also critical to elongated cell migration and are each regulated by dynamin [13, 20, 21]. Finally, dynamin plays a role in the activation of Arp2/3 [22] that is required for actin filament branching and membrane extension at the leading edge [23]. Collectively, these data suggest that dynamin may play a role in regulating elongated 3D migration.

To study dynamin in cellular functions there is now available an array of small molecules targeting different aspects of dynamin function, including Ryngo 1-23 (2-cyano-*N*-{3-[2-cyano-3- (3,4,5-trihydroxyphenyl) acryloylamino]propyl}-3-(3,4,5 trihydroxyphenyl) acrylamide) (previously named Bis-T-23 [24]). The inhibitory activity of Ryngo 1-23 that solely occurs *in vitro* [24] is contrasted with effects reported *in vivo*. In cells, Ryngo 1-23 has been demonstrated to promote dynamin oligomerization and thus stimulate the basal GTPase activity of dynamin [12]. Specifically, Ryngo 1-23 stimulates actin-dependent dynamin oligomerization at the cell's leading edge, in the transition zone between the lamellipodium and the lamellae, where the molecular clutch between actin and adhesion is engaged [12]. Thus, Ryngo 1-23 is a useful agent for investigating the role of actin-dependent dynamin oligomerization in cellular processes [12]. In the present study we have used Ryngo 1-23 to investigate the function of dynamin in 3D cell migration.

2. Materials and Methods

2.1 Cell culture, antibodies and reagents

Rat neuroblastoma (B35), human glioblastoma (U87MG), and human fibrosarcoma (HT1080) cell lines were maintained in Dulbecco's Modified Eagles Medium (DMEM) (Invitrogen) supplemented with 10% Foetal Bovine Serum (FBS). Growth of cells in 3D collagen gels and media for live imaging has been previously described [11]. MMP-2 pro- and active enzymes (Calbiochem, Merck) were used as positive controls for zymography. Stock solution of Ryngo® 1-23 [25] and Dynole® 34-2 [26] were prepared in DMSO.

2.2 Live cell imaging, migration analysis and collagen gel contraction

Cells were seeded in 3D collagen gels (1.7 mg/ml) in 24 well plates at a density of 3 x 10^5 cells per ml with 500µl of cell/collagen solution per well. Collagen was polymerised for at least 1 hour prior to the addition of 1 ml of DMEM containing 10% FBS. Following overnight incubation, complete media was exchanged for 500µl of serum-free DMEM containing dynamin targeting compounds. DMSO in all controls and drug-treated wells was maintained at 1% v/v. Following incubation at 37ºC for 30 minutes cultures were supplemented with an equal volume of CO_2-independent media containing 10% FBS for live cell imaging. Time-lapse images were captured over a period of 5 hours using an ORCA ERG cooled CCD camera (Hamamatsu, SDR Clinical Technology NSW, Australia) and an Olympus IX81 inverted microscope (Olympus) equipped with an environmental chamber heated to 37ºC. Transmitted light images were captured using a 20X objective. Cells undergoing division or apoptosis were excluded from analyses. Nuclear translocation was tracked in time-lapse image stacks using Metamorph V6.3 software (Molecular Devices, Sunnyvale, CA, USA). Directional persistence was calculated from Mean Squared Displacement (MSD) of cells versus time as previously described [6]. Relative cell elongation was determined by measuring the longest cell axis at the beginning and at the end of time lapse imaging. Quantification of cell viability was performed by direct addition of 10µM propidium iodide to 3D cell cultures. Viable cells were identified by exclusion of propidium iodide. Analysis of collagen gel contraction was performed as previously described [27].

2.3 Confocal microscopy

U87MG cells seeded in 3D collagen gels were fixed with 4% paraformaldehyde in phosphate buffered saline (PBS) and then stained with fluorescently-tagged phalloidin. Cell nuclei were counter-stained with prolong gold containing DAPI (Molecular probes, Invitrogen) and examined using a FluoView FV1000 confocal microscope (Olympus, Walkersville, NY, USA) with a UPLSAPO 60_NA1.2 water-immersion lens. TRITC-phalloidin was detected with a 559 nm laser set at 16.5% and DAPI with a 405 nm laser set at 42%. Imaging was performed with a 10 ms/ pixel sampling speed. Images were captured at 1024x1024 pixel resolution at 0.5 µm intervals. Final micrograph images were prepared using Photoshop C2S (Adobe, San Jose, CA, USA).

2.4 MMP-2 zymography

Cell supernatants and pro- and active MMP-2 standards (Calbiochem, Darmstadt, Germany) were assayed for gelatinase activity using a zymography assay. Briefly, electrophoresis was performed on 10% SDS-PAGE containing 1 mg/mL gelatin. Gels were washed in 2.5% (v/v) Triton X-100 and incubated overnight at 37°C in enzyme activation buffer (50 mM Tris-HCl, 200 mM NaCl, 0.02% (v/v) Tween 20 and 5 mM $CaCl_2$, pH 7.3). Gels were stained with Coomassie blue solution, destained and MMP-2 activity visualized as clear bands on a dark background.

2.5 Clathrin-mediated endocytosis

Assay of clathrin-mediated endocytosis was performed in a 96-well plate format as described previously (Hill et al 2009). Briefly, cells were grown and incubated with the drugs or vehicle for 30 min prior to addition of A594-conjugated transferrin (Tfn-A594) for 8 min at 37^{o}C. Cell surface bound transferrin was removed by a low pH acid wash and the cells were then fixed with paraformaldehyde. Tfn uptake was quantitated using an automated acquisition and analysis system (ImageXpress Micro (IXM), Molecular Devices, Sunnyvale, CA, USA). The average integrated intensity of Tfn-A594 was determined and the data were expressed as percentage of control.

2.6 Statistical analysis

All error bars on graphs represent the standard error of the mean (S.E.M). Statistical comparison of two means was performed by using a Student's *t*-test, calculated using Excel (Microsoft, Redmond, WA, USA) and comparison of more than two means was performed using one-way ANOVA with Tukey's multiple comparison test, in Prism V4 software (GraphPad Software, La Jolla, CA, USA).

3. Results

3.1 Ryngo 1-23 inhibits glioblastoma 3D migration

The selected cell lines were the U87MG glioblastoma, B35 neuroblastoma and HT1080 fibrosarcoma cells, each of which has been shown to adopt the elongated migration mode in 3D collagen gels [11, 28]. We first compared the behaviour of each line in 3D culture. B35 cells extend a thick, leading edge protrusion that displays multiple spikey projections at the tip (Figure 1A & Supplementary movie 1). The trailing edge is typically rounded and the cell body frequently displays a peanut-shell shape, suggestive of cell body constriction by surrounding matrix fibres (Figure 1B arrow heads). The HT1080 cells have previously been reported to display a mixed morphology in 3D culture [29] and similarly in our culture conditions approximately 50% of HT1080 cells display an elongated phenotype [11]. The elongated HT1080 cells move through the gels extending long thin extensions at both the leading edge and trailing edges (Figure 1A). Matrix fibres in advance of the leading edge are pulled in the direction of the cell, as the cells appear to tug on the collagen fibres (Figure 1C, Supplementary movie 2). At the rear a migration track is seen, where the cell has degraded and rearranged the matrix as it has created a path (Figure 1C). The U87MG cells also extend a long thin leading edge projection, although, in contrast to the HT1080 elongated invasion morphology, the U87MG leading edge is frequently a single mono-polar extension and the trailing edge is rounded (Figure 1A & supplementary movie 3). Similar to the HT1080 cells, the U87MG cells also displace local collagen fibres and in both cell lines it is possible to visualize tracks where the matrix has been rearranged as a cell has passed through. The U87MG cells move most rapidly through the gel, with an average speed of 0.48 ± 0.03 μm/min, compared with 0.23 ± 0.01 μm/min and 0.25 ± 0.01 μm/min for the B35 and HT1080 cells, respectively. Moreover, not all cells in the population are motile with the percentage of motile cells ranging from 60% ± 16 (HT1080), 69% ± 0.9 (U87MG) and 71% ± 7.3 (B35). Collectively, these data reveal that although each cell line displays an elongated mode of invasion, there are differences in their response to the external matrix organization.

We next determined the effect of Ryngo 1-23, a compound that promote dynamin's natural propensity to oligomerise and which stimulates its basal GTPase activity [12], on the 3D migratory behaviour of each cell line. Analysis of time-lapse series of cells treated with increasing concentrations of Ryngo 1-23 revealed that the total percentage of motile cells was not significantly affected in either the B35 or HT1080 cells lines, at any concentration tested (Figure 2A). In contrast, the percentage of U87MG cells migrating at the highest concentration of Ryngo 1-23 tested was significantly reduced (Figure 2A). Moreover, Ryngo 1-23 caused a concentration-dependent reduction in U87MG 3D migration speed (Figure 2B), but not in the B35 or HT1080 cells (Figure 2B). U87MG cells treated with Ryngo 1-23 lost their elongated phenotype (Figure 3A). Quantitative analysis confirmed that cell elongation was significantly reduced at both 10 and 100 μM Ryngo 1-23 concentrations in U87MG cells (Figure 3A) but there was no change in the morphology of B35 or HT1080 cells at any concentration examined (Supplementary movies 1 and 2). The reduced migration and increased rounding in the U87MG cells was not due to apoptosis or changes in proliferation in response to Ryngo 1-23, as both apoptotic and mitotic cells were excluded from analyses (as determined by cell morphology). Separately, quantification of U87MG cell viability by propidium iodide dye exclusion revealed no difference in cell viability at the highest concentration of Ryngo 1-23 used in this study (Figure 3B). Notably, the motile Ryngo 1-23-treated cells use the same elongated migration mode as their control counterparts (Figure 3C

and Supplementary Movie 4, note that this movie is for double the length of time as the control cell shown in Supplementary Movie 3). In contrast the spherical cells are essentially non-motile (Supplementary Movie 5).

We next asked whether Ryngo 1-23 might also reduce the 3D migration of other glioblastoma cells. The SMA-560 mouse glioblastoma cells are similar to the U87MG cells in that they invade brain tissue *in vivo* [30] and are likely to employ similar invasion mechanisms. As observed with U87MG cells, the SMA-560 cells displayed a concentration-dependent reduction in 3D cell speed following treatment with Ryngo 1-23 (Figure 4A). Given that the untreated SMA-560 cells had similar speed to the B35 and HT1080 cells (0.2 ± 0.02 μm/min) we compared the movement of SMA-560 cells with these lines. Comparison of the Mean Squared Displacement (MSD) for each cell line revealed that both the B35 and HT1080 curves crossed over the SMA-560 MSD curve, indicating that the SMA-560 cells move with increased directional persistence (Figure 4B). This behaviour is emphasized by analysis of paths traced by the SMA-560 and B35 cells. While the SMA-560 tended to more consistently move in the one direction, the B35 cells frequently changed direction, moving back over the same area (Figure 4C). Calculation of the persistence confirmed that the SMA-560 are significantly more directionally persistent than either the B35 or HT1080 cells (Figure 4D). This data indicates that despite the similar overall speed between the B35, HT1080 and SMA-560 cells, they employ different strategies to move through the 3D gels. Moreover, similar to the U87MG cells, SMA-560 elongation was reduced in the highest concentration of Ryngo 1-23 used (Figure 4E).

3.2 Ryngo 1-23 does not affect MMP activity or clathrin-mediated endocytosis

A switch from elongated to rounded cell morphologies in 3D collagen gels has previously been shown to occur in response to the inhibition of matrix metalloprotease (MMP) activity [29]. As dynamin regulates the pro-MMP-2 conversion to active MMP via delivery of membrane-type MMP-1 to the cell surface [19] and MMP-2 activity is associated with glioblastoma migration and invasion [31, 32], we asked whether the rounded phenotype and reduced migration speed might reflect Ryngo 1-23 effects on MMP activity. Analysis of MMP-2 activity by gelatin zymography revealed that there was no significant difference in the amount of secreted pro-MMP-2 in cells treated with Ryngo 1-23 when compared with matched controls (Figure 5A and B). Although levels of the active form of MMP-2 were too low for accurate quantification by densitometry, in 3 separate experiments faint bands were observed and no differences seen between control cell cultures versus cultures exposed to Ryngo 1-23 (Figure 5A). Therefore Ryngo 1-23 does not alter U87MG 3D migration via inhibition of MMP-2 function.

Dynamin also mediates clathrin-mediated endocytosis, which is a critical determinant of cell migration. Therefore we analyzed Ryngo 1-23 effects on endocytosis in the U87MG cells, using brief uptake of fluorescently-labeled transferrin in response to increasing concentrations of drug. No significant inhibition was detected, with only ~20% maximal inhibition observed at the highest concentration used (Figure 6A). For comparison, we also analyzed the effect of Ryngo 1-23 on transferrin uptake in B35 cells and found that Ryngo 1-23 also did not inhibit endocytosis in these cells (~20% maximal inhibition, Figure 6A). The efficacy of the transferrin endocytosis assay was independently confirmed using the well characterised dynamin inhibitor Dynole^{TM} 34-2 that has previously been shown to inhibit clathrin-mediated endocytosis [33]. Dynole 34-2 efficiently inhibited endocytosis in both the

U87MG (IC_{50} of 34.5 ± 10.8 µM) (Figure 6B) and B35 cells (IC_{50} of 6.6 ± 2.6 µM) (Figure 6B). Therefore Ryngo 1-23 inhibition of U87MG 3D migration is not due to inhibition of endocytosis.

3.3 Ryngo 1-23 alters glioblastoma adhesion to the matrix

Based on the emerging role for dynamin in regulating the actin cytoskeleton [12], we next considered whether the altered cell morphologies in response to Ryngo 1-23 might reflect changes in actin filaments. Prominent bundles of filamentous actin were observed at the lateral edges of extending membrane processes and in trailing processes in control U87MG cells (Figure 7A). In addition, thin, short actin filaments were observed extending into the leading edge of the extending membrane process. In contrast, significantly fewer U87MG cells displayed extended protrusions at concentrations of > 10 µM Ryngo 1-23 (Figure 7A). Instead, these spheroid-shaped cells frequently displayed actin-rich microspikes emanating from all over the cell body (Figure 7A). 3D projections of the phalloidin-stained cells emphasizes the differences in actin organization between control cells and cells exposed to Ryngo 1-23 (Supplementary movie 6). The actin cytoskeleton is intimately involved in the adhesion of the cells to the matrix and the migrating U87MG cells display prominent tugging on the matrix fibre. Therefore we asked whether the actin cytoskeleton changes following exposure to Ryngo 1-23 might reflect a change in the contractile force exerted by the cells through adhesion to the matrix. To test this we performed a collagen contraction assay (Figure 7B). This revealed significantly reduced gel contraction at 100 µM Ryngo 1-23 (Figure 7C). Using propidium iodide staining we confirmed that the reduced contractility was not due to an increase in apoptosis (Figure 6D). Together this suggests that Ryngo 1-23 treatment of U87MG reduces the adhesive forces that the cells exert on the surrounding matrix.

4. Discussion

Accumulating studies have suggested that dynamin may be an important target for the development of anti-invasive therapies for metastatic cancer [17, 18, 34]. Due to the increasing understanding of how cancer cells can adopt a range of migratory strategies to negotiate complex 3D extra-cellular environments [1] it is critical to use 3D culture methods to investigate the efficacy of compounds for blocking cancer cell migration and invasion. The results of our study demonstrate that the small molecule dynamin modulator Ryngo 1-23 suppresses the 3D cell migration speed of the glioblastoma cell lines U87MG and SMA-560. Our findings confirm that dynamin indeed plays a role in cell negotiation of a 3D extra-cellular environment.

Comparison of the 3D migration behaviours of the B35 neuroblastoma, HT1080 fibrosarcoma and U87MG cells revealed important differences. Analysis of the B35 cells revealed constriction by the local collagen fibres. Similar phenotypes were infrequently seen in the HT1080, SMA-560 and U87MG cells. Moreover, while the B35 cells also tugged on the fibres ahead of the cell, fibre displacement was much less than that observed with the other two cell lines. This suggests a greater adhesion to the surrounding matrix fibres by both the HT1080 and U87MG cells. The fact that the U87MG cell speed is almost double that of the HT1080 cells further suggests that these cells exert an even greater adhesive force on the surrounding fibres than the HT1080 cells. Previous studies have also revealed differences between the behaviour of U87MG and HT1080 cells in 3D collagen [28]. While the SMA-560 move more slowly than the U87MG cells, the enhanced directional persistence when compared with the B35 and HT1080 cells indicates a stronger adhesive force in these cells. Since Ryngo 1-23 inhibited 3D migration of U87MG (fast and persistent) and SMA-560 (persistent) cells, we propose that the compound preferentially inhibits migration that depends on strong adhesion to the extra-cellular matrix.

We tested known dynamin functions to determine whether these functions could account for Ryngo 1-23 inhibition of 3D migration and induce rounding. The changes are not due to apoptosis, MMP inhibition nor clathrin-mediated endocytosis. It was surprising that Ryngo 1-23 did not inhibit transferrin uptake, as previous studies have shown Ryngo 1-23 inhibits transferrin uptake in dendritic cells [35]. The differences may reflect the bulk endocytosis assay based on FACS used in the latter study, rather than the better characterised acute CME assay used here. Cell type specificity may also play a role, given that the dendritic cells are professional scavengers. Alternatively, the difference may reflect concentration-specific effects. While 100 μM Ryngo 1-23 was sufficient to inhibit endocytosis in dendritic cells [35] but not in U87MG cells, it is possible that higher concentrations of the compound may inhibit U87MG endocytosis. Nonetheless, since significant inhibition of 3D migration speed occurred at concentrations as low as 1 μM, inhibition of endocytosis cannot be the cause of reduced 3D migration in U87MG cells. Therefore Ryngo 1-23 inhibits U87MG motility by a mechanism that is unrelated to dynamin's function in endocytosis.

Dynamin plays a role in remodelling actin filaments and thereby influencing global actin cytoskeletal structure via either indirect mechanisms including interactions with cortactin [36] and regulating the disassembly of focal adhesions that anchor actin filaments [21, 37], or directly by interacting with short actin filaments to stimulate their uncapping and elongation [13]. Dominant negative dynamin, deficient in the binding and hydrolysis of GTP, is known

to alter both cell shape and cytoskeletal structure, causing a redistribution of stress fibres to the cell periphery [38]. Further, contractility of the actomyosin cytoskeleton is required for cells to exert force through the associated focal adhesions onto the surrounding matrix in order to translocate the cell body [39]. Our data reveal that Ryngo 1-23 induces altered actin arrangement and a corresponding reduction in the associated adhesive force to the extra-cellular matrix. Potentially, this reflects reduced ability of the cells to extend new membrane in order to form new adhesions to matrix fibres ahead of the cell. Rac GTPase-mediated activation of Arp2/3 is critical to the generation of short branched actin filaments that push the membrane forward [23]. It is therefore interesting that Rac inhibition differentially affects HT1080 versus U87MG cell 3D invasion [28]. While Rac inhibition induces amoeboid transition in HT1080 cells, U87MG cells instead display repressed actin polymerization at the tips of leading edge membrane protrusions. Our data reveals that Ryngo 1-23 specifically inhibits the elongated, directional mode of 3D migration exhibited by the U87MG and SMA-560 cells. Notably, a recent study using dynamin triple knockout cells revealed that the effects of one dynamin inhibitor compound include at least one off-target effect [40]. Thus it remains possible that Ryngo 1-23 may be affecting other targets. However, the off-target issue is not a problem limited to the use of small molecules as cell biology probes. The problem is potentially more significant in genetically manipulated cells where transfections and/or knockdowns occur for days instead of minutes, and have many off-target actions on other proteins which can be down-regulated [41] or mislocalised in the cell [40]. Nonetheless, Ryngo 1-23 has been shown to induce actin-dependent dynamin oligomerization at the cell's leading edge [12] and dynamin regulates the actin/adhesion molecular clutch at the leading edge [16]. Thus we propose that Ryngo 1-23 modulates the actin/adhesion clutch, thus reducing the transmission of the acto-myosin force required for elongated, persistent movement in a 3D environment.

Our study has revealed that the dynamin modulating small molecule Ryngo 1-23 significantly inhibits U87MG and SMA-560 glioblastoma cell 3D migration speed. Collectively, our data reveal an important non-endocytic function for dynamin in 3D cell migration, but suggests a specific role in the elongated cell invasion that depends on the formation of actin stress fibres required to transmit cellular force in order to move through the 3D matrix.

Acknowledgements

This study was supported by NSW Cancer Council grant RG12/06 (GO) and National Health and Medical Research Council grants 512251 and 632515 (GO) and 1032771 (PJR and AM), the Brain Cancer Discovery Collaborative supported by Cure Brain Cancer Foundation (GO), University of Sydney grant 2010-02657 (GO), Cancer Australia/Cure Cancer Foundation grant (JL) and a University of Sydney Thompson Fellowship (AA). Equipment was supported by grants from the Cancer Institute NSW, The Australian Cancer Research Foundation and the Ramaciotti Foundation. Ryngo®, Dynole™ and MiTMAB™ are trademarks of Children's Medical Research Institute and Newcastle Innovation Ltd. Ryngo® 1-23, Dynole™ 34-2 and MiTMAB are available from Abcam (Cambridge, UK).

References

[1] V. Sanz-Moreno, C.J. Marshall, The plasticity of cytoskeletal dynamics underlying neoplastic cell migration, Curr. Opin. Cell Biol. 22 (2010) 690-696.

[2] P. Friedl, Prespecification and plasticity: shifting mechanisms of cell migration, Curr. Opin. Cell Biol. 16 (2004) 14-23.

[3] M.L. Kutys, A.D. Doyle, K.M. Yamada, Regulation of cell adhesion and migration by cell-derived matrices, Exp. Cell Res. 319 (2013) 2434-2439.

[4] P. Bradbury, B. Fabry, G.M. O'Neill, Occupy tissue: The movement in cancer metastasis, Cell Adhesion & Migration, 6 (2012) 424-432.

[5] M. Menon, D.A. Schafer, Dynamin: expanding its scope to the cytoskeleton, Int. Rev. Cell Mol. Biol. 302 (2013) 187-219.

[6] C.T. Mierke, D. Rosel, B. Fabry, J. Brabek, Contractile forces in tumor cell migration, Eur. J. Cell Biol. 87 (2008) 669-676.

[7] C.T. Mierke, B. Frey, M. Fellner, M. Herrmann, B. Fabry, Integrin alpha5beta1 facilitates cancer cell invasion through enhanced contractile forces, J. Cell Sci. 124 (2011) 369-383.

[8] K. Hu, L. Ji, K.T. Applegate, G. Danuser, C.M. Waterman-Storer, Differential transmission of actin motion within focal adhesions, Science. 315 (2007) 111-115.

[9] R.J. Petrie, N. Gavara, R.S. Chadwick, K.M. Yamada, Nonpolarized signaling reveals two distinct modes of 3D cell migration, J. Cell Biol. 197 (2012) 439-455.

[10] C.T. Bach, S. Creed, J. Zhong, M. Mahmassani, G. Schevzov, J. Stehn, L.N. Cowell, P. Naumanen, P. Lappalainen, P.W. Gunning, G.M. O'Neill, Tropomyosin isoform expression regulates the transition of adhesions to determine cell speed and direction, Mol. Cell Biol. 29 (2009) 1506-1514.

[11] J.G. Lees, C.T.T. Bach, P. Bradbury, A. Paul, P.W. Gunning, G.M. O'Neill, The actin-associating protein Tm5NM1 blocks mesenchymal motility without transition to amoeboid motility, Oncogene. 30 (2011) 1241-1251.

[12] C. Gu, J. Chang, V.A. Shchedrina, V.A. Pham, J.H. Hartwig, W. Suphamungmee, W. Lehman, B.T. Hyman, B.J. Bacskai, S. Sever, Regulation of Dynamin Oligomerization in Cells: The Role of Dynamin-Actin Interactions and Its GTPase Activity, Traffic. 15 (2014) 819-838.

[13] C. Gu, S. Yaddanapudi, A. Weins, T. Osborn, J. Reiser, M. Pollak, J. Hartwig, S. Sever, Direct dynamin-actin interactions regulate the actin cytoskeleton, EMBO J. 29 (2010) 3593-3606.

[14] S. Sever, J. Chang, C. Gu, Dynamin rings: not just for fission, Traffic. 14 (2013) 1194-1199.

[15] G.L. Razidlo, Y. Wang, J. Chen, E.W. Krueger, D.D. Billadeau, M.A. McNiven, Dynamin 2 potentiates invasive migration of pancreatic tumor cells through stabilization of the Rac1 GEF Vav1, Dev. Cell. 24 (2013) 573-585.

[16] M. Menon, O.L. Askinazi, D.A. Schafer, Dynamin2 organizes lamellipodial actin networks to orchestrate lamellar actomyosin, PloS one. 9 (2014) e94330.

[17] H. Yamada, T. Abe, S.A. Li, Y. Masuoka, M. Isoda, M. Watanabe, Y. Nasu, H. Kumon, A. Asai, K. Takei, Dynasore, a dynamin inhibitor, suppresses lamellipodia formation and cancer cell invasion by destabilizing actin filaments, Biochem Biophys Res Commun. 390 (2009) 1142-1148.

[18] R.D. Eppinga, E.W. Krueger, S.G. Weller, L. Zhang, H. Cao, M.A. McNiven, Increased expression of the large GTPase dynamin 2 potentiates metastatic migration and invasion of pancreatic ductal carcinoma, Oncogene. 31 (2012) 1228-1241.

[19] A. Jiang, K. Lehti, X. Wang, S.J. Weiss, J. Keski-Oja, D. Pei, Regulation of membrane-type matrix metalloproteinase 1 activity by dynamin-mediated endocytosis, Proc Natl Acad Sci U S A. 98 (2001) 13693-13698.

[20] E.J. Ezratty, M.A. Partridge, G.G. Gundersen, Microtubule-induced focal adhesion disassembly is mediated by dynamin and focal adhesion kinase, Nat. Cell Biol. 7 (2005) 581-590.

[21] Y. Wang, H. Cao, J. Chen, M.A. McNiven, A direct interaction between the large GTPase dynamin-2 and FAK regulates focal adhesion dynamics in response to active Src, Mol. Biol. Cell. 22 (2011) 1529-1538.

[22] D.A. Schafer, S.A. Weed, D. Binns, A.V. Karginov, J.T. Parsons, J.A. Cooper, Dynamin2 and cortactin regulate actin assembly and filament organization, Curr. Biol. 12 (2002) 1852-1857.

[23] T.D. Pollard, Regulation of actin filament assembly by Arp2/3 complex and formins, Ann Rev Biophys. Biomol. Structure. 36 (2007) 451-477.

[24] L.R. Odell, N. Chau, A. Mariana, M.E. Graham, P.J. Robinson, A. McCluskey, Azido and diazarinyl analogues of bis-tyrphostin as asymmetrical inhibitors of dynamin GTPase, Chem. Med. Chem. 4 (2009) 1182-1188.

[25] T. Hill, L.R. Odell, J.K. Edwards, M.E. Graham, A.B. McGeachie, J. Rusak, A. Quan, R. Abagyan, J.L. Scott, P.J. Robinson, A. McCluskey, Small molecule inhibitors of dynamin I GTPase activity: development of dimeric tyrphostins, J. Med. Chem. 48 (2005) 7781-7788.

[26] T.A. Hill, C.P. Gordon, A.B. McGeachie, B. Venn-Brown, L.R. Odell, N. Chau, A. Quan, A. Mariana, J.A. Sakoff, M. Chircop, P.J. Robinson, A. McCluskey, Inhibition of dynamin mediated endocytosis by the dynoles--synthesis and functional activity of a family of indoles, J. Med. Chem. 52 (2009) 3762-3773.

[27] J.G. Lees, Y.W. Ching, D.H. Adams, C.T. Bach, M.S. Samuel, A.J. Kee, E.C. Hardeman, P. Gunning, A.J. Cowin, G.M. O'Neill, Tropomyosin regulates cell migration during skin wound healing, J. Invest Dermatol. 133 (2013) 1330-1339.

[28] D. Yamazaki, S. Kurisu, T. Takenawa, Involvement of Rac and Rho signaling in cancer cell motility in 3D substrates, Oncogene. 28 (2009) 1570-1583.

[29] K. Wolf, I. Mazo, H. Leung, K. Engelke, U.H. von Andrian, E.I. Deryugina, A.Y. Strongin, E.B. Broecker, P. Friedl, Compensation mechanism in tumor cell migration: mesenchymal-amoeboid transition after blocking of pericellular proteolysis, J. Cell Biol. 160 (2003) 267-277.

[30] T.T. Tran, M. Uhl, J.Y. Ma, L. Janssen, V. Sriram, S. Aulwurm, I. Kerr, A. Lam, H.K. Webb, A.M. Kapoun, D.E. Kizer, G. McEnroe, B. Hart, J. Axon, A. Murphy, S. Chakravarty, S. Dugar, A.A. Protter, L.S. Higgins, W. Wick, M. Weller, D.H. Wong, Inhibiting TGF-beta signaling restores immune surveillance in the SMA-560 glioma model, Neuro-oncology. 9 (2007) 259-270.

[31] S.K. Chintala, R. Sawaya, Z.L. Gokaslan, J.S. Rao, Modulation of matrix metalloprotease-2 and invasion in human glioma cells by alpha 3 beta 1 integrin, Cancer Lett. 103 (1996) 201-208.

[32] S.K. Chintala, J.C. Tonn, J.S. Rao, Matrix metalloproteinases and their biological function in human gliomas, Int. J. Dev. Neurosci. 17 (1999) 495-502.

[33] M.J. Robertson, F.M. Deane, P.J. Robinson, A. McCluskey, Synthesis of Dynole 34-2, Dynole 2-24 and Dyngo 4a for investigating dynamin GTPase, Nat. Protocols. 9 (2014) 851-870.

[34] H.P. Joshi, I.V. Subramanian, E.K. Schnettler, G. Ghosh, R. Rupaimoole, C. Evans, M. Saluja, Y. Jing, I. Cristina, S. Roy, Y. Zeng, V.H. Shah, A.K. Sood, S. Ramakrishnan, Dynamin 2 along with microRNA-199a reciprocally regulate hypoxia-inducible factors and ovarian cancer metastasis, Proc Natl Acad Sci U S A. 111 (2014) 5331-5336.

[35] K.J. Sandgren, J. Wilkinson, M. Miranda-Saksena, G.M. McInerney, K. Byth-Wilson, P.J. Robinson, A.L. Cunningham, A differential role for macropinocytosis in mediating entry of the two forms of vaccinia virus into dendritic cells, PLoS Pathogens. 6 (2010) e1000866.

[36] O.L. Mooren, T.I. Kotova, A.J. Moore, D.A. Schafer, Dynamin2 GTPase and cortactin remodel actin filaments, J. Biol Chem. 284 (2009) 23995-24005.

[37] W.T. Chao, J. Kunz, Focal adhesion disassembly requires clathrin-dependent endocytosis of integrins, FEBS Lett. 583 (2009) 1337-1343.

[38] H. Damke, T. Baba, D.E. Warnock, S.L. Schmid, Induction of mutant dynamin specifically blocks endocytic coated vesicle formation, J. Cell Biol. 127 (1994) 915-934.

[39] A.J. Ridley, M.A. Schwartz, K. Burridge, R.A. Firtel, M.H. Ginsberg, G. Borisy, J.T. Parsons, A.R. Horwitz, Cell migration: integrating signals from front to back, Science. 302 (2003) 1704-1709.

[40] R.J. Park, H. Shen, L. Liu, X. Liu, S.M. Ferguson, P. De Camilli, Dynamin triple knockout cells reveal off target effects of commonly used dynamin inhibitors, J. Cell Sci. 126 (2013) 5305-5312.

[41] S.M. Ferguson, A. Raimondi, S. Paradise, H. Shen, K. Mesaki, A. Ferguson, O. Destaing, G. Ko, J. Takasaki, O. Cremona, O.T. E, P. De Camilli, Coordinated actions of actin and BAR proteins upstream of dynamin at endocytic clathrin-coated pits, Dev. Cell. 17 (2009) 811-822.

Legends

Figure 1. Elongated 3D migration. (A) Bright-field time-lapse images of B35, HT1080 and U87MG cells in 3D collagen gels. Time shown in hours and minutes. Scale bar 50 μm. (B) B35 cell showing cell body constriction (arrow heads). (C) HT1080 cell showing the displacement of collagen fibres at the leading edge (blue lines) and the migration track at the trailing edge (green arrow heads).

Figure 2. Ryngo 1-23 inhibits U87MG 3D migration. (A) Percentage of motile cells in the different cell types under the indicated conditions. Graph shows the mean of three independent experiments. (B) Average cell speeds. Data show the average of four independent experiments, n~30 cells tracked per condition, per experiment. *p<0.05, **p<0.01, ***p<0.001.

Figure 3. Ryngo 1-23 reduces U87MG elongation. (A) Bright field time-lapse series of U87MG cells in 3D collagen gel, time shown in minutes after treatment with Ryngo 1-23. Histogram shows elongation ratios (expressed relative to controls) following 5 hours of treatment with the indicated concentrations of Ryngo 1-23. Elongation ratios were measured by comparing cell length at zero time point to cell length after 5 hours treatment with Ryngo 1-23. Data are the mean values from three independent experiments. *p<0.05. (B) Viability of U87MG cells was unaffected by Ryngo 1-23 exposure as measured by propidium iodide dye exclusion following 5 hours treatment with either control DMSO media or 100 μM Ryngo 1-23. (C) Motile cells retain an elongated phenotype, but move more slowly through the gel. Montage shows U87MG cells treated with 10μm Ryngo 1-23.

Figure 4. Ryngo 1-23 inhibits 3D migration of SMA-560 glioblastoma cells. (A) Average SMA-560 cell speeds in the indicated concentrations of Ryngo 1-23. Data show the average of four independent experiments, n~30 cells tracked per condition, per experiment. (B) MSD calculated from the trajectories of U87MG, SMA-560, B35 and HT1080 cells in 3D collagen gels. Data are the average values from at least 4 independent experiments, n=30 cells tracked per experiment. (C) Examples of the migration tracks taken by SMA-560 and B35 cells. Each time point is indicated by a white spot and the distance travelled between consecutive time point is indicated by the joining lines. Shown are examples of 15 individual cells from each cell line. (D) B35 and HT1080 cells are significantly less directionally persistent than SMA-560. (E) Elongation ratios (expressed relative to controls) following 5 hours of treatment with the indicated concentrations of Ryngo 1-23. (D) *p<0.05, **p<0.01, ***p<0.0001, NS=not significant.

Figure 5. Cell rounding is not due to inhibited MMP-2 activity. (A) Gelatin zymography of MMP-2. Gels were loaded with purified pro-MMP-2 (both the pro- and active forms are visible, lane 1) and active MMP-2 (lane 2). MMP-2 levels in conditioned media with 1% DMSO and cell-free collagen gels in the absence and presence of 100 μM Ryngo 1-23 are shown in lanes 3 and 4, respectively. Lanes 5 and 6 show MMP-2 in conditioned media from collagen gels containing U87MG cells in the absence and presence of 100μM Ryngo 1-23, respectively. Similar low level active MMP2 (lanes 5 and 6) was seen in three independent experimental repeats, but levels were too low for densitometric analysis. (B) Graph showing densitometric analysis of pro-MMP-2 levels under the indicated conditions, expressed relative to levels in the control. Bars show the average from three independent experiments. **p<0.01, NS = not significant.

Figure 6. Ryngo 1-23 does not inhibit clathrin-mediated endocytosis. (A) Quantification of labelled transferrin uptake at the indicated concentrations of Ryngo 1-23 in U87MG and B35 cells. (B) Labelled transferrin uptake following exposure to Dynole 34-2 as indicated. Error bars represent SEM of three independent experiments, each performed in triplicate.

Figure 7. Ryngo 1-23 disrupts the actin cytoskeleton and reduces collagen gel contraction. (A) Percentage of spheroid shaped U87MG cells. Micrographs show examples of cells that were fixed, permeabilized and stained with fluorescently-labelled phalloidin to detect filamentous actin. Arrowheads in control cells indicate actin filaments (stress fibres) in the body of the elongated cell and along the cell perimeter. Arrowheads in Ryngo 1-23 indicate actin-rich microspikes. (B) Collagen gel contraction assay. Images show examples of gels containing U87MG cells released from the wells and then incubated for 5 days. Arrows indicate gel diameters. (C) Area of released collagen expressed relative to area of gel in the absence of drug. ***$p<0.001$, one-way ANOVA with Tukey's post-comparison test.

Supplementary Movie 1. Brightfield timelapse of B35 cells within 3D collagen gels, under control conditions (left panel) or treated with 100 μM Ryngo 1-23 (right panel).

Supplementary Movie 2. Brightfield timelapse of HT1080 cells within 3D collagen gels, under control conditions (left panel) or treated with 100 μM Ryngo 1-23 (right panel).

Supplementary Movie 3. Brightfield timelapse of U87MG cells within 3D collagen gels (total time 4 hrs and 53 mins).

Supplementary Movie 4. Brightfield timelapse of U87MG cells within 3D collagen gels treated with 100 μM Ryngo 1-23 (total time 7 hrs and 24 mins).

Supplementary Movie 5. Example of rounded U87MG cells treated with 100 μM Ryngo 1-23.

Supplementary Movie 6. Z-projections of phalloidin stained U87MG cells seeded within 3D collagen gels and treated with control media or Ryngo 1-23 as indicated.

Figure
Click here to download high resolution image

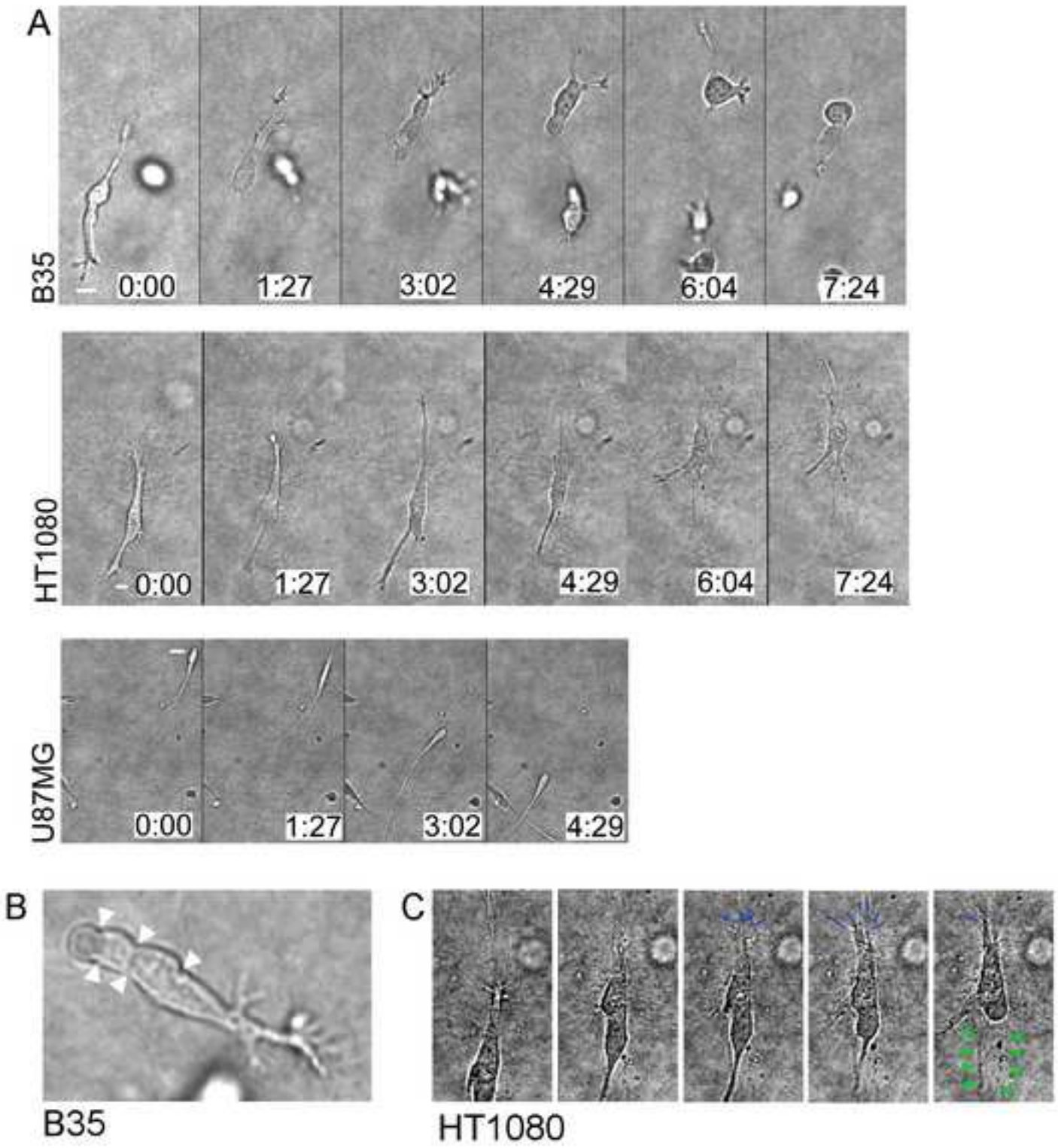

Figure 2

Click here to download high resolution image

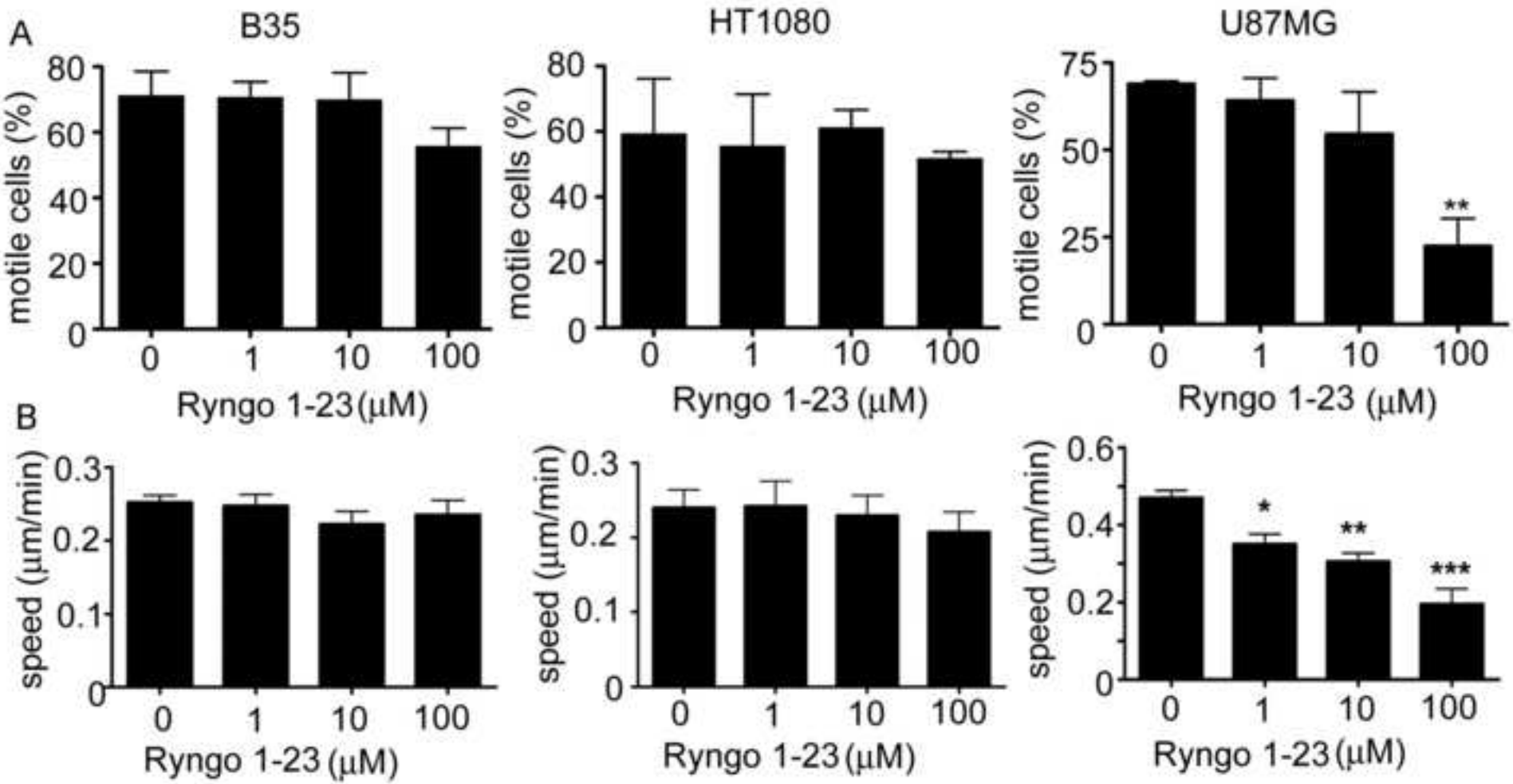

Figure 3

Click here to download high resolution image

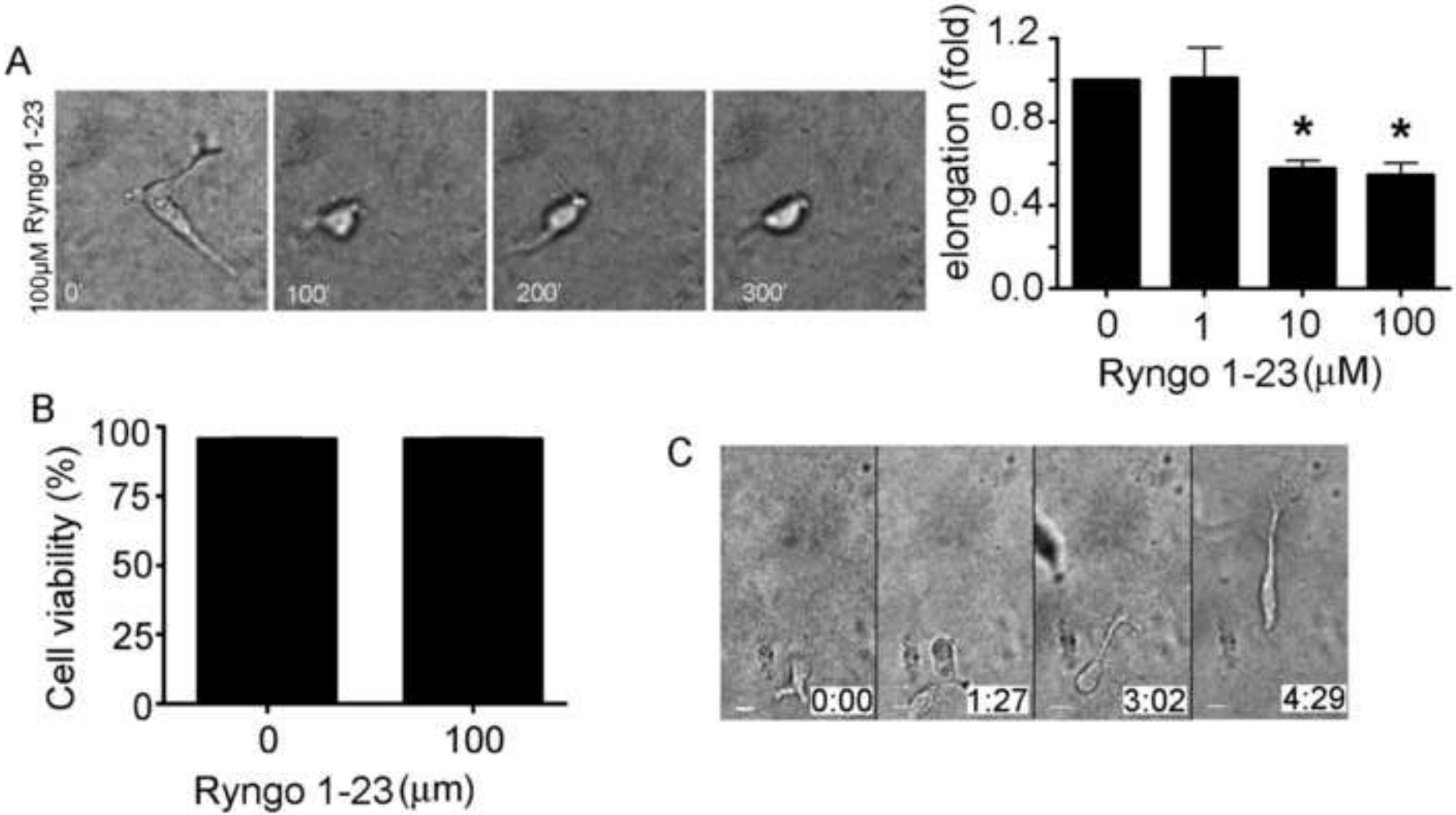

Figure 4

Click here to download high resolution image

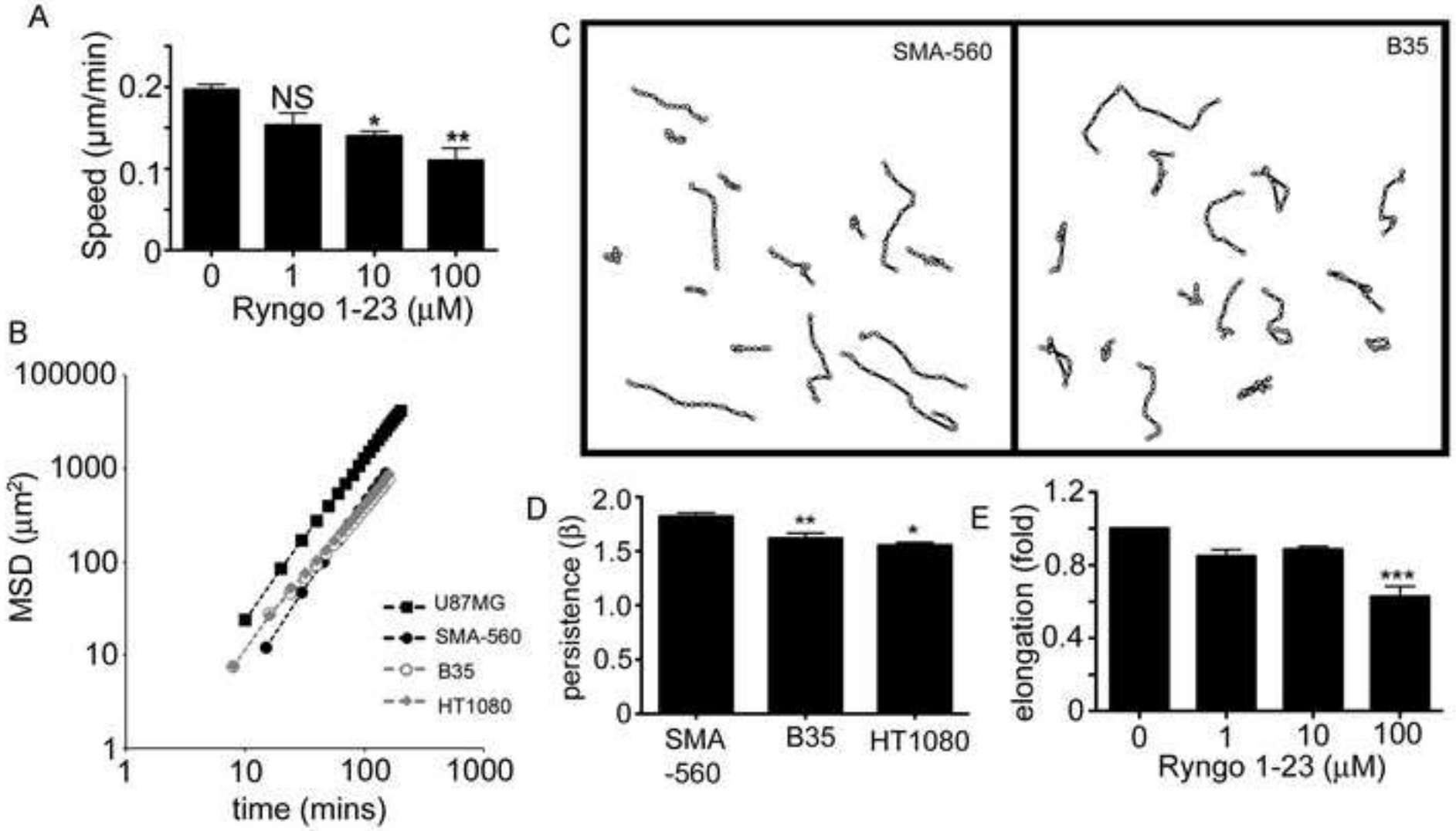

Figure 5

Click here to download high resolution image

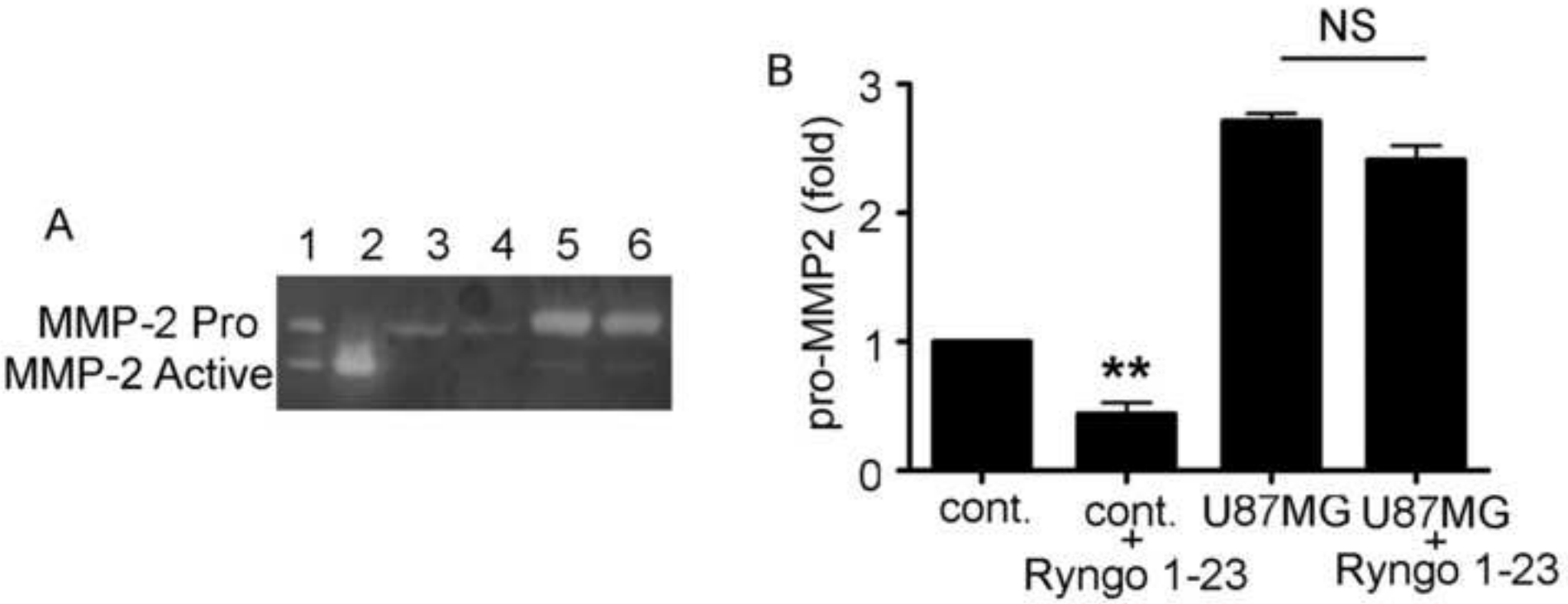

Figure 6

Click here to download high resolution image

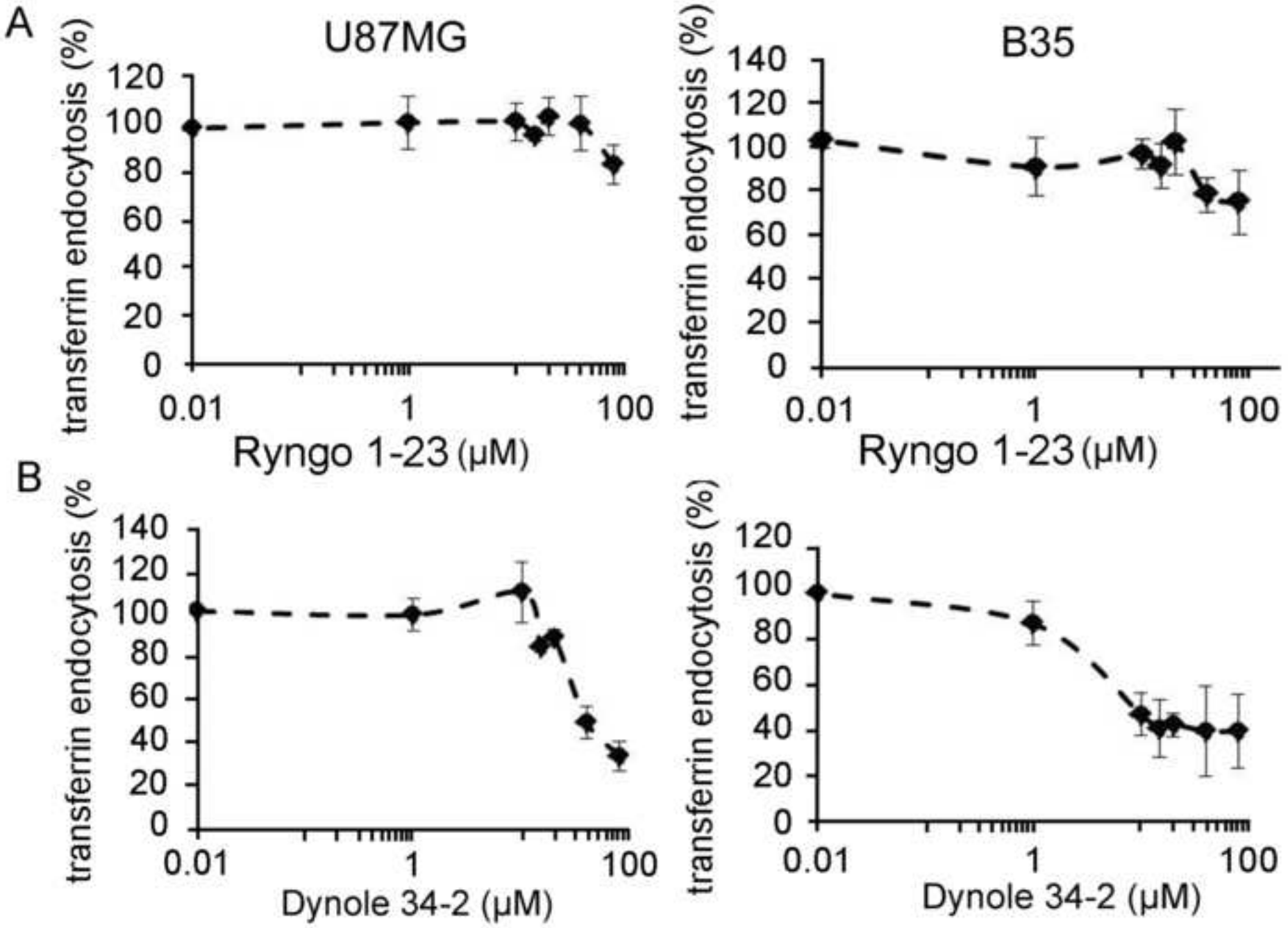

Figure 7

Click here to download high resolution image